

This article may be downloaded for personal use only. Any other use requires prior permission of the author and AIP Publishing. This article appeared in J. Chem. Phys. 147, 024706 (2017) and may be found at <https://doi.org/10.1063/1.4991344> and <https://aip.scitation.org/doi/10.1063/1.4991344>

Exploring the Driving Forces behind the Structural Assembly of Biphenylthiolates on Au(111)

Elisabeth Verwüster¹, Elisabeth Wruss¹, Egbert Zojer¹, and Oliver T. Hofmann^{1}*

1 Institute of Solid State Physics, NAWI Graz, Graz University of Technology, Petersgasse 16,
8010 Graz, Austria

***Corresponding Author:** Oliver T. Hofmann, o.hofmann@tugraz.at

Abstract

In this contribution we use dispersion-corrected density functional theory to study inter- and intramolecular interactions in a prototypical self-assembled monolayer (SAM) consisting of biphenylthiolates bonded to Au(111) via thiolate groups. The goal is to identify the nature of the interactions that drive the monolayer into a specific conformation. Particular focus is laid on sampling realistic structures rather than high symmetry model configurations. This is achieved by studying conceptually different local minimum structures of the SAM that are obtained via exploring the potential energy surface from systematically varied starting geometries. The six obtained packing motifs differ in the relative arrangement of the two molecules in the unit cell (coplanar *versus* herringbone) and in the intramolecular configuration (twisted *versus* planar rings). We find that van-der-Waals interactions within the organic adsorbate and between adsorbate and substrate are the main reason that these molecular assemblies can form stable structures at all. The van-der-Waals interactions are, however, very similar for all observed motifs; by analyzing various types of interactions in the course of three notional SAM-formation steps we find that the main driving force stabilizing the actual global minimum structure originates from electrostatic interactions between the molecules.

KEYWORDS Self-assembled monolayer, binding energy, metal/organic interface, density functional theory, band-structure calculation, interface simulation, SAM-formation process, van-der-Waals interactions, π -stacking.

Introduction

Surface modification via organic self-assembled monolayers (SAMs) provides a versatile technique to tune the properties of metal substrates, with important technological applications e.g. in organic electronic devices,¹⁻⁸ as corrosion protection,⁹ and as active material in bio-sensing.^{10,11} The impact of the SAM on the system properties does not depend solely on the chemical structure of the molecule. Rather, also the way the molecules arrange on the surface, i.e. the polymorph the SAM adopts, plays a decisive role.¹²⁻²⁰

Presently, very little is known about the relation between molecular structure and the formed adsorption motif,²¹⁻²³ or the nature of the interaction that relate these two. Also in computational studies the surface polymorph that is eventually found significantly depends on the chosen initial geometry prior to geometry optimization and on numerical details, such as the initialization of the Hessian.²² The corresponding properties of interest can, however, vary significantly depending on which structure is found.^{12,25}

In this work, we employ density-functional theory to investigate the energy landscape of the prototypical biphenylthiolate SAM on Au(111). The focus is not so much on systematically calculating every possible polymorph structure, but rather on what type of interactions are crucial for stabilizing/destabilizing a specific configuration and how these interactions depend on the specific arrangement of the molecules. Here, the various conceptually different adsorption motifs identified in our structure search serve as ideal, realistic test structures for performing that comparison.

The investigated system is illustrated in Figure 1. Biphenylthiol derivatives bonded to the Au surface via thiolate docking groups are frequently used as models to demonstrate the physical

effects at work at SAM/Au interfaces.^{26–33,13,34–36} We will show in the following that even for such a comparably simple system, a variety of intermolecular and intramolecular arrangements are conceivable, for which fundamental differences in the different types of interaction energies can be expected. These are explored by defining a hypothetical SAM-formation process occurring in several well-defined steps (molecular deformation, self-assembly, and bonding to the substrate, see below). In this way we find that, although van-der-Waals interactions are the main driving force for SAM formation, electrostatic interactions between the molecular backbones determine what is the most stable surface polymorph.^{37–41}

Methodology

Computational details

The band-structure calculations in this work employed dispersion-corrected density functional theory using a modified version of the Vienna Ab-Initio Simulation Package⁴² (based on VASP version 5.4.1, see below for more details). Throughout this work, the Perdew-Burke-Enzerhof (PBE)^{43,44} exchange-correlation functional was applied together with “standard” projected augmented-wave (PAW) potentials^{45,46} to treat core-valence interactions. To account for long-range dispersion forces (vdW), the PBE functional was augmented by the Tkatchenko-Scheffler scheme⁴⁷ parameterized specifically to treat adsorption on metallic surfaces (PBE+vdW^{surf}).⁴⁸ The vdW-correction between the atoms of the Au substrate was switched off.

A cutoff energy of 400 eV for the plane waves and a 8x5x1 Monkhorst-Pack⁴⁹ type k-point mesh were used. To model the self-assembled monolayer on the metallic substrate, we applied the

repeated slab approach. Decoupling of the periodic replicas of the slab was achieved by inserting a 20 Å vacuum gap and a self-consistently determined dipole layer compensating for the electrostatic asymmetry.⁵⁰ While systematically exploring the potential energy surface of biphenylthiolate on Au(111), the gold surface was represented by a 3-layer slab to reduce computational cost. Calculations for the notional SAM-formation were done with a 5-layered slab for a higher accuracy. Test calculations show a difference of 15-60 meV in the total adsorption energy between the 3-layered and 5-layered slab (see Table S1 in the Supporting Information). To avoid spurious surface reconstructions, the Au(111) lattice constant was set to the equilibrium value for the used methodology, which amounts to 2.928 Å. An optimization scheme based on internal coordinates and the Direct Inversion in the Iterative Subspace (DIIS)⁵¹ algorithm as implemented in the GADGET tool²⁴ was used to relax the geometries. The top two layers of the slab and the molecules were allowed to relax until the remaining forces were smaller than 10^{-2} eV/Å and tight convergence criteria of 10^{-6} eV were employed for the SCF (self-consistent field) procedure.

The vibrational analysis was done via “analytical frequencies”, i.e. employing density-functional perturbation-theory (DF-PT) including vdW-corrections, which was kindly implemented into our modified VASP version by Tomáš Bučko. For these calculations, the dipole correction was switched off, as it caused a strong (artificial) imaginary frequency corresponding to a translational mode towards the correcting dipole layer. More details regarding the computational settings for the vibrations can be found in the Supporting Information.

For gas-phase calculations of the isolated molecules, the geometry in the gas-phase was obtained via pre-optimization with Gaussian09⁵² using the PBE functional and the 6-311++G** basis set

and subsequently placing the molecule in a $40 \text{ \AA} \times 40 \text{ \AA} \times 40 \text{ \AA}$ unit cell to obtain a consistent energy within VASP.

Results and discussion

System set-up

Our study focusses on a self-assembled monolayer of biphenylthiolates adsorbed on Au(111). Biphenyl(thiole) suggests itself for the present study, since it is well known to exhibit a strongly twisted conformation in the gas-phase ($\gamma \approx 45^\circ$)⁵³ while as bulk material, the twist angle is strongly reduced (typically to 10° or less).^{54–56,53,57,58} In other words, the twist angle between the rings is a clear source for structural variations.

On the surface, scanning tunneling microscopy (STM)^{20,59,60} experiments propose a herringbone arrangement of the bonded biphenylthiolate molecules. Typically, the STM tips cannot penetrate the material deep enough to yield authoritative information on the planarity. Still, DFT calculations imply that the molecules ought to be planar, which has been attributed to spatial constraints due to the presence of the Au surface.⁵⁶ As we show in this paper, for biphenylthiolate changes in the tilt as well as variations in the relative arrangement of the molecules in the unit cell indeed result in several possible, locally stable motifs on the surface.

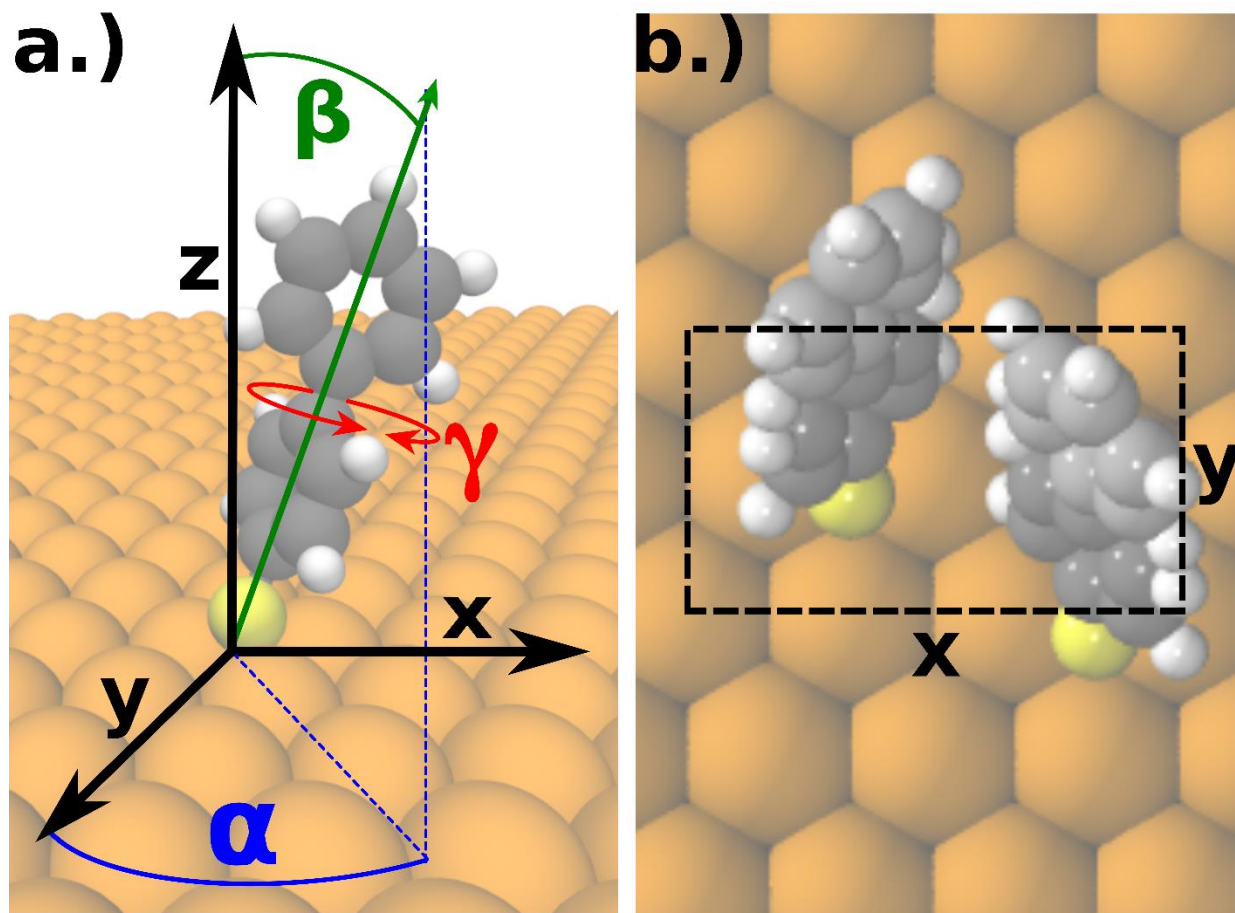


Figure 1: a) schematic representation of the angles, which have been modified for generating a variety of starting configurations; the tilt angle, β , between the long molecular axis and the z-axis of the unit cell, the inter-ring twist, γ , between the top and bottom phenyl ring of the biphenthylthiolate molecule, and the azimuthal angle, α , between the y-axis of the unit cell and the projection of the long molecular axis onto the surface plane. b) top view of the $3 \times \sqrt{3}$ unit cell containing two molecules. White spheres correspond to H, grey to C, yellow to S and gold to Au atoms.

To assess the structural diversity of biphenthylthiolates on Au(111), we systematically explored the potential energy surface (PES) of the metal/organic interface. We focus our efforts on the $c(3 \times \sqrt{3})$

unit cell containing two molecules, which is the unit cell commonly found in experiments for oligophenylene-thiolates on Au(111) at full coverage.^{18,20,59} Although studying the PES for other supercells would be highly interesting, performing an exhaustive search that explores the huge diversity of potential supercells at the same time as the potential inter- and intramolecular interactions is presently not tractable and would also go beyond the scope of the present paper.

To explore the PES, a set of suitable starting geometries (140 in total) was generated by varying the following three structural parameters (also shown in Fig. 1a):

- (i) The azimuthal angle, α , which determines the intermolecular arrangement of the two biphenylthiolates in the unit cell. It is defined as the angle between the projection of long molecular axis of the molecule onto the gold surface and the y-axis of the unit cell. Given the orthogonal orientation of the unit cell vectors, we scan this angle between 0° and 90° in steps of 30° .
- (ii) The tilt angle, β , between the long molecular axis and the z-axis of the unit cell. Experimental NEXAFS-studies suggest a tilt of $27 \pm 5^\circ$.⁶¹ To capture as many conformations as possible, we scanned β in the range between 0° and 45° in steps of 15° . Larger tilt angles are not sensible due to the dense packing at full coverage and would result in unphysical interpenetration of the molecules. The tilt angle was either set symmetrically, i.e., with both molecules tilted in the same direction, or alternatingly, with the two molecules in the unit cell tilted in opposite directions.
- (iii) The inter-ring twist angle, γ , between the two rings in each biphenyl backbone between -90° and 90° in steps of 45° . The need to investigate γ at positive and negative values originates from having two non-equivalent biphenyl moieties in the unit cell. We chose this particular range for γ to fully include the competition between the repulsion of the

ortho-substituted hydrogens (that would be minimized for $\gamma = 90^\circ$) and the drive for maximizing π -conjugation (that would be maximized for $\gamma = 0^\circ$.^{62,53})

Unless otherwise noted, all geometric changes were applied in parallel to both molecules in the unit cell. Out of 140 starting geometries generated this way, we discarded 45 structures because they would be either symmetry equivalent to other configurations or unphysical due to an interpenetration of the molecules. Subsequently, the remaining 95 geometries were relaxed towards the nearest local minimum for 20 optimization steps. The target of this pre-optimization is to determine the nearest “catch-basin”, i.e., the nearest minimum structure, as indicated in Figure 2a. We note in passing that after these 20 steps, the maximum residual force has fallen below 10^{-1} eV/Å (but not reached the final convergence criterion of 10^{-2} eV/Å), indicating that all these structures are already reasonably close to a structural minimum geometry. Visual inspection of the geometry after this “pre-relaxation” allows to systematically capture the structural diversity of the SAM and to identify the key packing motifs that we need in a second step to analyze the relevance of the different interactions at work in the SAMs.

Already at the “pre-relaxation” stage it becomes clear that not all starting geometries head towards the planar herringbone structure, which is the motif typically suggested by experiments.^{18,20,59,60} Consequently, all pre-relaxed geometries are categorized depending on (a) whether the molecules are planar or twisted, and (b) whether the top, respectively, bottom rings of the two molecules pack in a co-planar or herringbone arrangement. This gives rise to six different primary structural categories. Throughout this paper, each category is named according to the relative arrangement of the upper and lower phenyl rings of the two molecules in the unit cell (herringbone denoted as **HB** and co-planar denoted **CP**). Additionally, we determined the inter-ring twist angle in each

molecule; here, *0*, indicates that both molecules are planar, *1*, signifies that one molecule is non-planar, and *2* denotes a situation in which both molecules are twisted. To assess the planarity, we defined a threshold of $\gamma < 20^\circ$ after the first 20 steps of the optimization. In the final nomenclature the structural parameters are then separated by a slash. In this way, *HB/HB/0*, for example, denotes two planar molecules, where both phenyl rings are arranged in a herringbone fashion. A schematic sketch of all six motifs, along with the relative energy of all group members, is given in Figure 2b.

We emphasize that although the energies of the non-converged geometries are not quantitatively reliable; as mentioned above, they are already close to, but not yet at a minimum geometry. Still, it is noteworthy that only 43% of the starting structures converge towards a *HB/HB/0* structure, while a significant portion (31%) falls into the attractor basin of *HB/HB/2*; i.e. they result in herringbone patterns of non-planar molecules. The other categories are significantly less populated as the remaining (26%) starting structures spread across the other four motifs. These results imply that the herringbone-arrangement is particularly robust with respect to the starting geometry guess, whereas the outcome whether the molecules assume a planar or twisted geometry is more sensitive.

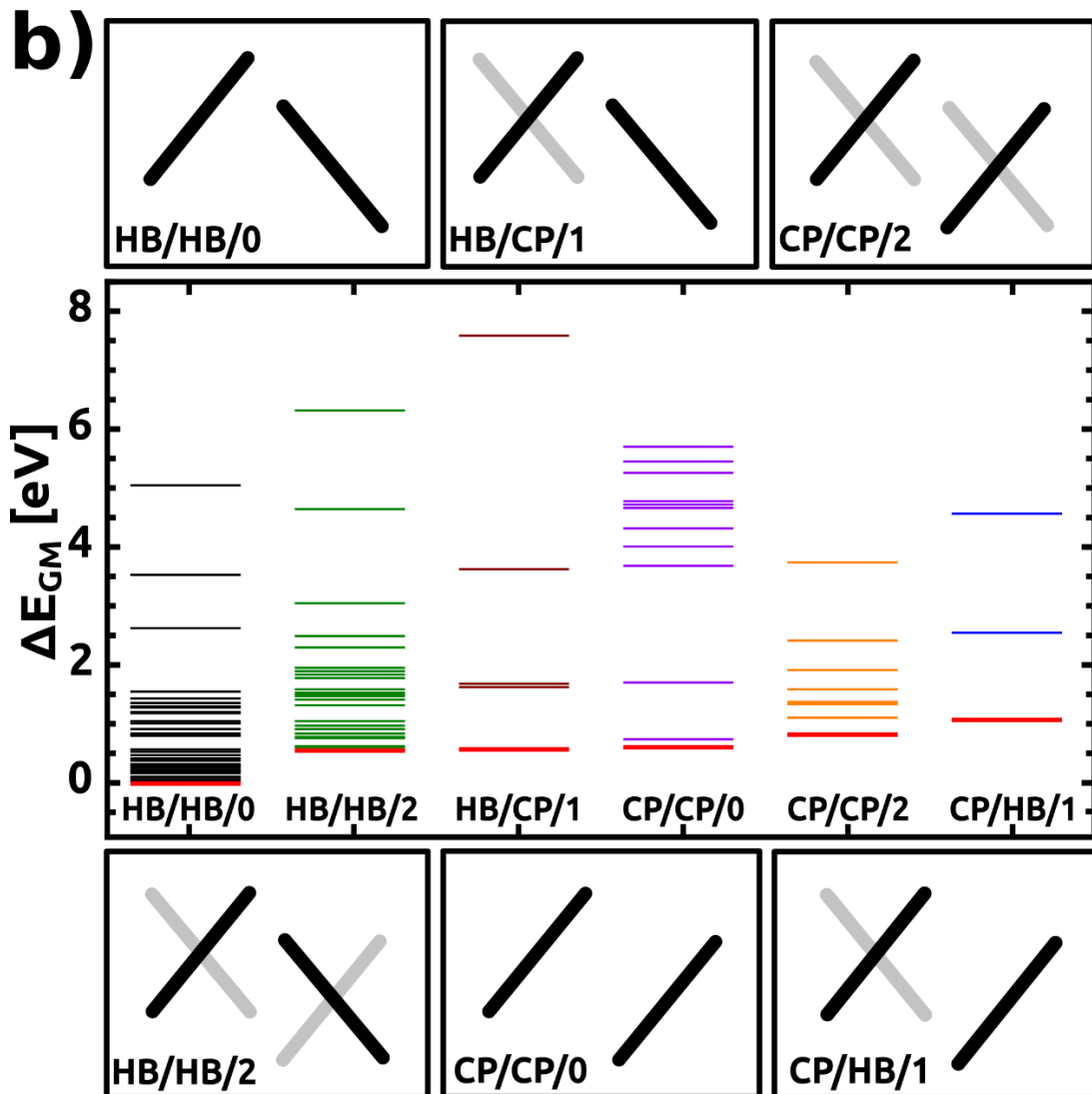
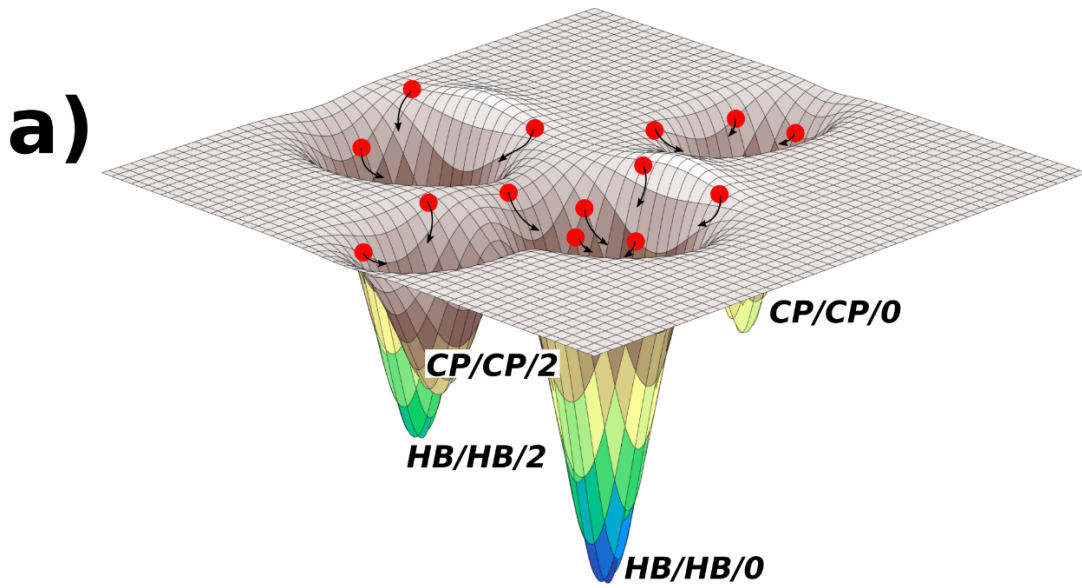


Figure 2: a) Schematic potential energy surface presenting the four local minima of the motifs HB/HB/0, HB/HB/2, CP/CP/0 and CP/CP/2. The red dots illustrate a set of starting geometries with their trajectories (black arrows) towards the closest local minima basin. b) Energy of all calculated (not converged) geometries categorized in the six main motifs. Structures within the same categories may vary in the arrangement with respect to the surface normal. The red lines correspond to the energy of the obtained minimum after the final relaxation of the corresponding motif, as discussed in detail in the main text. The panels above and below the plot contain schematic sketches of the six categories with the upper (lower) phenyl ring drawn in black (gray) and the naming convention (HB = herringbone, CP = co-planar, 0/1/2 = number of inter-ring twists per unit cell).

The low-energy members of each category differ typically only regarding the orientation within the unit cell, i.e. with respect to α . Here, we postpone the question of whether this leads to different local minima or whether the orientation with respect to the surface is a comparably weak degree of freedom which takes particularly long to optimize. Rather, we focus on the conceptually different packing motifs, as they serve as ideal test structures for analyzing different contributions to the SAM bonding. Therefore, we selected the energetically lowest lying pre-optimized geometry of each motif and performed a full relaxation until the remaining forces were smaller than 10^{-2} eV/Å. Finally, a vibrational analysis is performed in order to ascertain that all final geometries correspond to local minima. Whether and to which extent vibrational spectroscopy could be used as tool to determine the motif experimentally is discussed in the Supporting Information. We note that the vibrational zero-point energies between the different categories do not differ notably (less than 50 meV, see Table 1), and are, therefore, not considered further. (Although inclusion of the

zero-point energy changes the relative ordering of HB/CP/1 and CP/CP/0, the difference is small and this effect is not relevant for the further discussion). The geometries of the obtained minima of each of the six categories are shown in Figure 3.

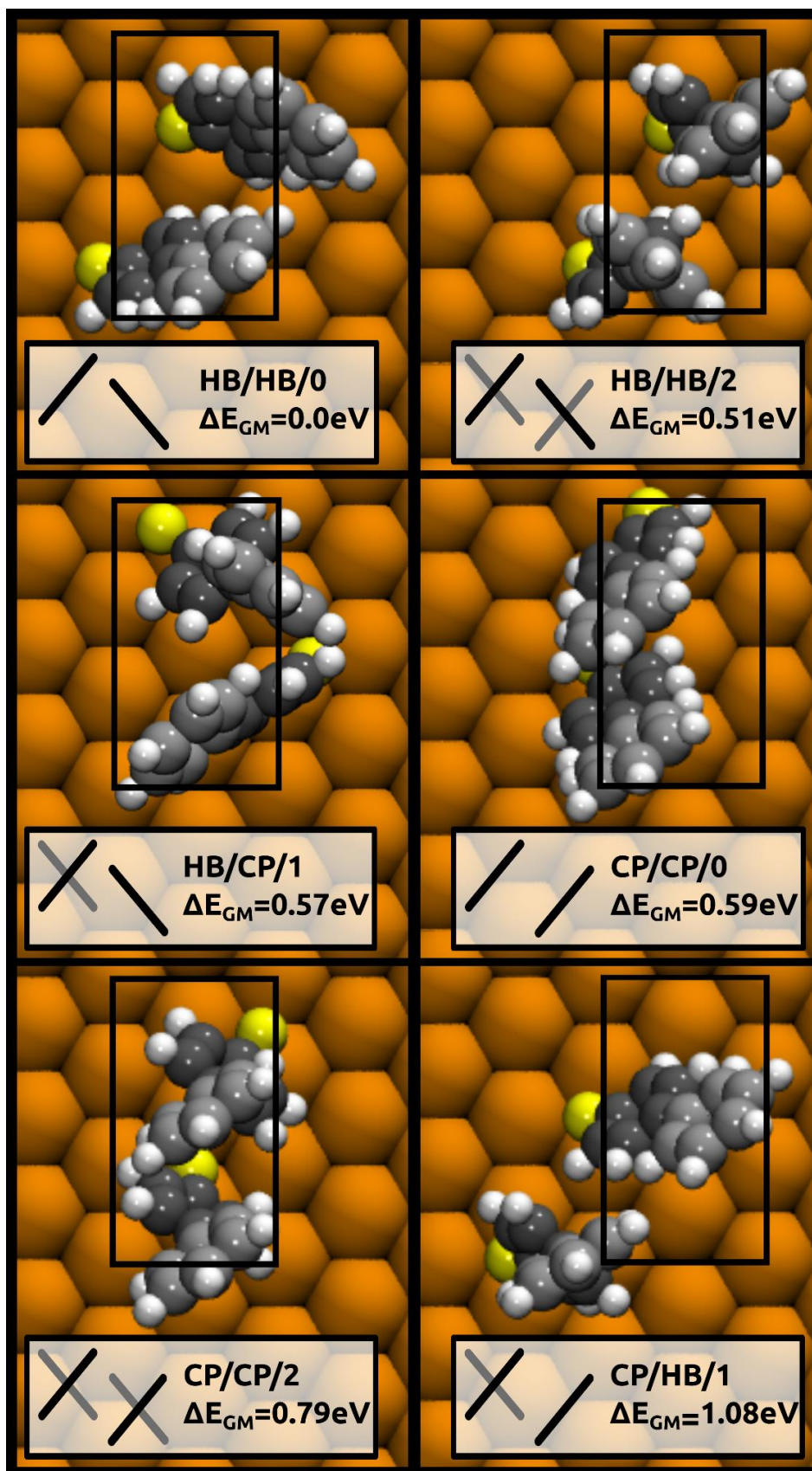


Figure 3: Top view of the obtained minimum geometries for each category. The insets contain the naming convention (*HB* = herringbone, *CP* = co-planar, 0/1/2 = number of inter-ring twists per motif), the energy, ΔE_{GM} , relative to the lowest energy found in this study (*HB/HB/0*) and a schematic illustration of each motif. For the sake of clarity, only the two molecules that constitute the unit cell (black rectangle) are shown, and neighboring molecules are omitted.

As a general observation, the obtained geometries of the motifs are either almost perfectly planar or strongly twisted with $\gamma \approx 70\text{-}80^\circ$. Notably, the latter twist angle is much larger than the equilibrium γ found in the gas-phase.^{63–65} Furthermore, we find that motifs with planar molecules are much more tilted ($\beta \approx 30^\circ$) than twisted ones ($\beta \approx 15^\circ$), for reasons that will become evident later in this work. As expected, *HB/HB/0* is the most stable category. All other structures are 0.5–1.0 eV higher in energy. In thermodynamic equilibrium they would, therefore, be hardly occupied. Nevertheless, it is useful to analyze the different local minimum structures in more detail, as they allow generating fundamental insight into the interactions that are responsible for the bonding within SAMs and that stabilize certain configuration compared to others.

Ranking the six categories according to the total energies of the obtained minima, we find the following order (from most to least stable): *HB/HB/0* > *HB/HB/2* > *HB/CP/1* > *CP/CP/0* > *CP/CP/2* > *CP/HB/1* (see Table 1). This suggests that the relative arrangement of the upper phenyl rings is the most crucial parameter. It also implies that a T-shaped arrangement of neighboring rings resulting in a herringbone pattern is preferred over a co-planar situation. The second aspect is the twist of the two biphenyls in the unit cell: For a given motif of the upper ring, both molecules being planar (0) is more stable than both twisted (2), and either is significantly more stable than

having one molecule twisted and one planar (1). Importantly, what we do not observe is that the planar structures are generally more stable than the twisted ones.

Table 1: Tilt-, inter-ring twist- and azimuthal angles α , β , and γ of the lowest energy structures of the six main structural motifs in order of increasing total energies. The zero-point corrected energy, ΔE_{GM} , and the zero-point energy, ΔZPE_{GM} , are given relative to the energy of the global minimum system HB/HB/0.

Category	azimuth, α [°]	tilt, β [°]	inter-ring twist, γ [°]	Relative energy, ΔE_{GM} [meV]	Relative zero-point energy, ΔZPE_{GM} [meV]
HB/HB/0	0	28	0	0	0
HB/HB/2	1	13	80	512	-45
HB/CP/1	5	13/32	75/0	566	-17
CP/CP/0	72	25	0	585	-37
CP/CP/2	71	21	70	787	-34
CP/HB/1	25	23/38	80/0	1080	2

Analyzing the interactions in the various configurations

An obvious question at this point is what causes the notable energy differences between the various polymorphs, in particular whether they originate from the geometric distortion of the molecules, the intermolecular interactions in the organic layer, or the adsorption of the organic material onto the metallic substrate. In order to investigate the physical aspects that drive the SAMs into specific structures, we, therefore, designed a gedankenexperiment splitting the SAM formation into three fundamental steps:

Starting from the isolated, fully optimized biphenylthiole molecule in the gas-phase, we calculate (i) the energy related to the deformation of the free molecules into the geometry they exhibit in the SAM, i.e. the “deformation energy”, ΔE^{deform} , (ii) the energy required to assemble the deformed but isolated molecules into the periodic monolayer, i.e., the assembly energy, $\Delta E^{assembly}$, and (iii) the energy associated with the reaction of the free-standing monolayer with the surface, i.e. the adsorption energy, ΔE^{ads} . By definition, positive values indicate an endothermic, negative values an exothermic process. For this analysis, we omit the HB/CP/1 and CP/HB/1 polymorphs that contain two qualitatively different molecules, which would complicate the following analysis without providing notable additional insight.

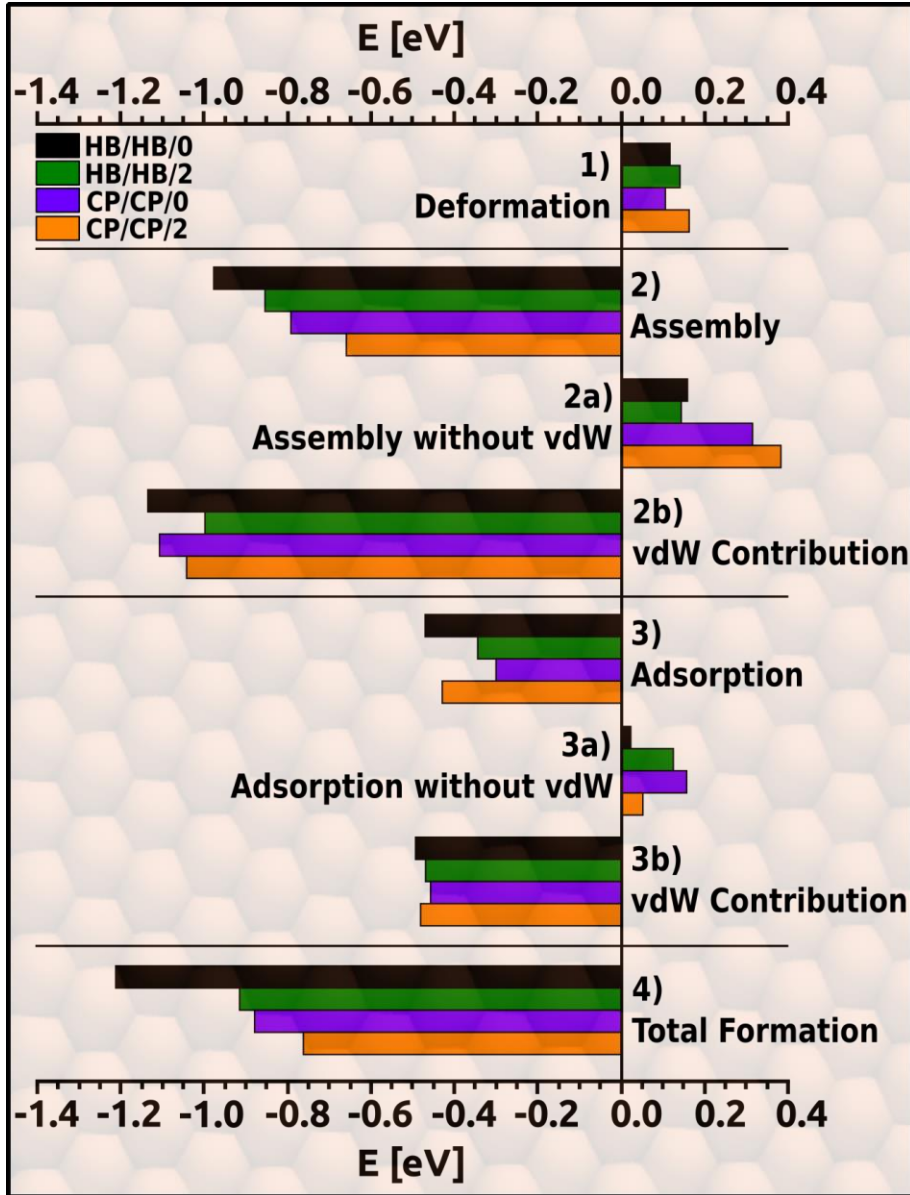


Figure 4: SAM-formation process split into separate contributions: 1) deformation energy, ΔE^{deform} ; 2) assembly energy, $\Delta E^{assembly}$; 2a) assembly energy without vdW correction; 2b) vdW contribution to the assembly process, ΔE^{vdW} ; 3) adsorption energy, ΔE^{ads} ; 3a) adsorption energy without vdW correction; 3b) vdW-contribution to ΔE^{ads} ; and 4) the sum of all contributions, ΔE^{total} , for the different local minimum structures HB/HB/0 (black), HB/HB/2 (green), CP/CP/0 (purple) and CP/CP/2 (orange).

Step 1: Molecular deformation

To illustrate the energetic cost of deforming the molecule from its gas-phase geometry to the monolayer-induced geometry, ΔE^{deform} , we calculate the energy difference

$$\Delta E^{deform} = E_{mol,mon} - E_{mol,gp} \quad (1)$$

where $E_{mol,gp}$ is the energy of an optimized molecule in its gas-phase conformation ($\gamma = 40^\circ$); $E_{mol,mon}$ denotes the energy of a molecule forced into the geometry it adopts in the monolayer. The difference was calculated for both molecules in the unit cell separately. The final ΔE^{deform} represents the average value for the two molecules of the unit cell (the individual values can be found in the Supporting Information, Table S2).

As shown in Figure 4, the motifs formed by planar molecules, HB/HB/0 and CP/CP/0, show smaller deformation energies compared to the twisted HB/HB/2 and CP/CP/2 (ca. 20 meV and 60 meV, respectively), indicating that it is slightly *less* costly to planarize the single molecule than to enlarge its inter-ring twist. This seems to contradict literature where it has been suggested that planarizing biphenyl is energetically more costly than twisting the rings by 90° .^{53,66} As the same energetic order prevails when substituting the SH group by H (while keeping the geometry otherwise constant (see Table S3 in the SI)), it is clear that this discrepancy is not related to the presence of the electron donating thiol group favoring a more planar conformation. Rather, we find that the origin for the “easier planarization” is a consequence of an interplay with other molecular degrees of freedom. When we allow the molecules to relax while fixing the monolayer-

induced twist angle between the phenyl rings, we restore the expected situation that twisting the rings is energetically less costly than planarizing them. The corresponding calculations can be found in the SI, Table S4.

This implies that the differences in deformation energy between different conformations are mostly due to geometry changes of the molecule other than twisting the rings. Such deformations are triggered by effects such as the tilting and close packing of the molecules. An even more important observation is that the energetic difference between planarization and twisting are overall rather small, which means that molecular deformations per se are *not* a major driving force favoring a specific polymorph. This also means that finding polymorphs with strongly twisted molecules is indeed a possibility that ought to be considered seriously in particular for molecules or unit cells somewhat differing from the present one. Indeed, in a recent study some of us observed that for the structurally related molecule phenyl-piperidine-dithiocarbamate (assembled on Au(111) in the same unit cell as chosen here) the planar and twisted conformations are energetically almost degenerate.⁶³

Step 2: Molecular assembly

Step 2 of our notational SAM-formation describes the assembly of isolated molecules, $E_{mol,mon}$, (already in the final structure) into an extended, free-standing monolayer with an energy E_{mon} . The corresponding energy, $\Delta E^{assembly}$, is given by:

$$\Delta E^{assembly} = 0.5 \cdot (E_{mon} - 2E_{mol,mon}) \quad (2)$$

In analogy to ΔE^{deform} , $\Delta E^{assembly}$ is first assessed for each of the two molecules in the unit cell separately, with the average value presented in Figure 4 (the individual values can be found in the Supporting Information, Table S5). We find that the energies range from -660 meV to -980 meV, i.e. interestingly, the differences (up to 320 meV) are much more pronounced for this step than for any other in our gedankenexperiment. Indeed, the variation in the assembly step is so large that the hierarchy observed here is preserved in the overall energy tally (step 4). This indicates that the intermolecular interaction within the layer is the most important contribution determining which structure the molecular adsorbate will eventually adopt.

This raises the question, to what extent the SAM structure is determined by van-der-Waals (vdW) interactions. To address that, we first discuss $\Delta E^{assembly}$ omitting vdW interactions (step 2a in Figure 4) and then evaluate the vdW contribution to $\Delta E^{assembly}$ (step 2b in Figure 4) separately. This facilitates the analysis and allows us to demonstrate that both components have fundamentally different impact on the energetics.

For the energy contributions *without* vdW forces, we find that all four systems are clearly repulsive (step 2a) with the repulsion for SAMs with molecules in herringbone arrangement being smaller by ~200 meV compared to the co-planar polymorphs. Within a given arrangement (HB or CP),

only a minor difference in energy is observed (~50 meV). This indicates that the arrangement of the backbones crucially affects the assembly energies, while the twisting of the biphenyls is insignificant.

Besides vdW interactions, the interactions between the molecules can conceptually be broken down into electrostatic interactions and interaction arising from the wave-function overlap. For closed-shell molecules, the latter is always repulsive as consequence of Pauli-repulsion. Its magnitude increases with increasing wave-function overlap. Although Pauli-repulsion is difficult to quantify from our calculations, qualitative insights into the differences between the polymorphs can be obtained via the band-structure of the free-standing monolayers (since also the band-dispersion directly depends on the wave-function overlap). The corresponding plots can be found in the SI (Figure S3). If Pauli-repulsion were the main factor influencing the assembly energy, we would expect a positive correlation between the band-dispersion and $\Delta E^{assembly}$ when disregarding vdW interactions. A comparison between Figure 4 and Figure S3, however, shows that such a correlation does not exist. In fact, the least repulsive structure, HB/HB/0, is the one that shows the largest band dispersion for both of its highest occupied bands (ca. 300 meV), while the bandwidth for the other structures tends to be smaller by about a factor of two. From these observations, we infer that the interaction between the molecules in the monolayer is strongly impacted by electrostatic effects.³⁴⁻³⁸

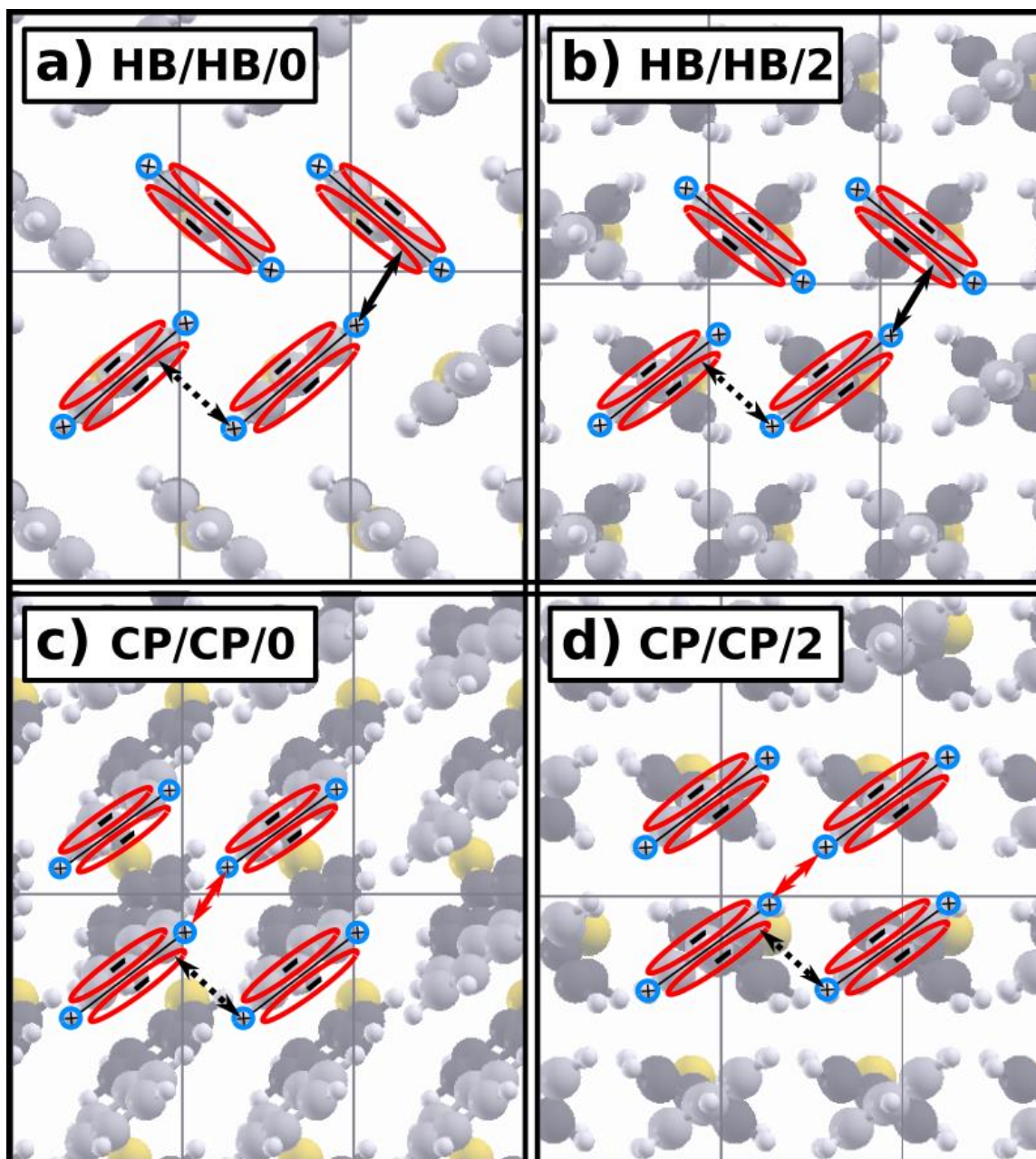


Figure 5: Schematic sketch of the biphenyl stacking variations occurring in the discussed motifs. The overlay, which illustrates the electrostatic interactions, references only to the upper phenyl rings, while the bottom rings are darkened as guide to the eye for illustrative purposes. T-shaped stacking is indicated with a black arrow, parallel-displaced stacking with a dashed arrow and “side-by-side” stacking with a red arrow for the motifs a) HB/HB/0, b) HB/HB/2, c) CP/CP/0 and d) CP/CP/2.

The electrostatic interaction between the biphenylthiole molecules originates from the interaction of the π -electron cloud above and below the molecular plane and the σ -framework (C-H bonds) at the rim of the molecule. In our SAM categories, we can identify three prototypical interaction motifs that are often discussed in literature in the context of aromatic interactions.³⁷⁻⁴¹ These are, as schematically indicated in Figure 5, T-shaped stacking, parallel-displaced stacking, and “side-by-side” stacking. All categories contain a combination of these stacking variations: The herringbone arranged structures exhibit both T-shaped and parallel-displaced stacking (see Fig 5a for HB/HB/0 and 5b for HB/HB/2). The co-planar arrangements mostly display parallel-displaced stacking along both the long and short axis of the unit cell, while there is a “side-by-side” stacking along the unit cell diagonal (see Fig 5c for CP/CP/0 and 5d for CP/CP/2).

From other studies on benzene dimers, it is known that T-shaped (edge-on structure) stacking is the most favorable arrangement.^{37-41,68,69} In this motif, the molecules are almost perpendicular to each other and the hydrogen atoms of one molecule point towards the π -cloud of the adjacent molecule. The parallel-displaced stacking is energetically only slightly worse.^{37,38} It consists of molecules that are horizontally shifted by ca. half the width of a molecule, such that the π -clouds of adjacent molecules avoid each other and come as close as possible to the hydrogen atoms. In contrast, “side-by-side” stacking, where the molecules are aligned such that the hydrogen atoms repel each other, is energetically very unfavorable.

These considerations suggest that it is in particular the presence of the repulsive “side-by-side” stacking in the co-planar motifs that render them energetically less favorable than their herringbone stacked siblings.

Nevertheless, the vdW forces are responsible for the overall attractive interactions associated with the monolayer-assembly, as illustrated in Step 2b, Figure 4. These interactions contribute more than 1.0 eV to the binding energy for all investigated motifs, which makes them the largest of the individual contributions considered here and renders them a major driving force for SAM formation. Between the different categories, we find that vdW energies are larger for planar than for the twisted molecules. The motifs with planar molecules are also the ones with increased tilt angles (see Table 1). This correlation is insofar reasonable, as the effective volume the molecules occupy decreases with increasing tilt. Consequently, SAMs consisting of more tilted molecules are more densely packed (assuming constant coverage), which results in a larger vdW attraction.

Step 3: Adsorption of the SAM

Adsorbing the hypothetical free-standing monolayer of biphenylthioles on the Au(111) surface, ΔE^{ads} , composes the third and last step in our gedankenexperiment describing SAM-formation. The saturated monolayer binds to the gold slab by substituting the thiole S-H bond for a covalent thiolate S-Au bond. We are aware that the fate of the hydrogen atoms has been controversially discussed in literature.⁷⁰ This, however, does not matter for the present discussion, since it only constitutes an equal energy offset for all motifs. For simplicity, we thus assume that the hydrogen leaves the surface as molecular hydrogen, H₂. Hence, the adsorption energy of the SAM per molecule, ΔE^{ads} , was calculated as the energy difference between the complete system, E_{sys} , and its separate building blocks, where E_{mon} is the energy of the free-standing monolayer, E_{Au} , the energy of the gold slab and E_{H_2} the energy of the hydrogen molecule.

$$\Delta E^{ads} = 0.5 \cdot \{E_{sys} - [E_{Au} + (E_{mon} - E_{H_2})]\} \quad (4)$$

Here we stress that the process described in Eq.(4) does not describe the formation of the bond between the thiolate and the Au surface, but rather quantifies the energy for replacing the covalent bond between S and H with a thiolate bond of the docking groups to the substrate (R-S-Au). In analogy to the SAM-formation discussed in the preceding section, when omitting vdW-contributions, ΔE^{ads} yields solely positive values (step 3a). Thus, without dispersion, no adsorption of the monolayer onto the surface would occur. The necessity of including vdW-correction even for covalently bonded SAMs has, in fact, already been reported previously.^{71,72,32,73,74} Interestingly, the magnitude of the vdW attraction towards the surface is essentially equal for all conformations (within approximately 40 meV), i.e. it does not particularly prefer any packing motif over another (step 3b).

Although the variation in the adsorption energies without vdW interactions is significantly larger (differing by up to ca. 100 meV, see step 3a in Figure 4), neither the intermolecular conformation (i.e., the planarity) nor the intramolecular arrangement (i.e., whether the molecules arrange HB or CP), seem to play a decisive role.

At this point the question arises whether the strong variation can be traced to either steric interactions between the monolayers and the gold substrate, or whether there is a notable difference in the chemical reactivity of thioles.

To answer that question, we calculated the energies (using Gaussian09, see above) associated with proton abstraction, i.e., the reaction



for each of the molecules in the unit cell separately fixing their geometries to the ones they adopted in the bonded SAMs (i.e., only the position of the H atom of PhPh-SH is relaxed). The reaction

described in Equ. (5) does not contain any steric interaction with the gold substrate and would be expected to yield essentially equal results, if the molecules were also electronically equivalent. Interestingly, we find that they are not. Rather already for this reaction we observe to us surprisingly large differences of up to 80 meV (see Table S6 in the SI). This means that not only the reactivity between the different categories differs, but even the two molecules in the unit cell can be chemically inequivalent. Indeed, this observation is also manifested in the band structure of the free-standing monolayers (see SI, Fig. S3), where the two highest occupied bands in all systems consist of states localized only on one of the molecules. Only in HB/HB/0, the shape of the two highest occupied bands is qualitatively equivalent, except for a small offset. For all other configurations, a strong asymmetry between the two bands can be found, corroborating the observed (electronic and chemical) asymmetry of the two molecules. We tentatively infer from these data that the different reactivity towards the substrate is mostly a consequence of the differing geometries of the monolayers. As discussed above, is the latter are to a large part determined by the interaction energies in the assembly process (see above).

Summary and conclusion

In the present paper we analyze the relative importance of a variety of interactions for the stability of different polymorphs of biphenylthiolates on Au(111). This system serves as a prototypical example for a strongly bonded metal-organic interface consisting of building blocks that allow for some flexibility regarding their internal structure as well as relative arrangement. To generate diverse polymorphs as ideal test systems for analyzing the interactions, we extensively explore the potential energy surface (PES) for a structure with two molecules in a $c(3\times\sqrt{3})$ unit cell identify six packing motifs with fundamentally different conformations. These differ in the planarity of the molecules and in the relative arrangement of the rings in coplanar or herringbone fashion.

To understand, which factors stabilize specific polymorphs over others, we discuss a hypothetical, albeit very insightful SAM-formation process consisting of: (i) molecular deformation, (ii) assembly of the molecules into a monolayer, and (iii) bonding of that monolayer to the substrate. Interestingly, although the conformations of the molecules massively differ in the different polymorphs, the energies necessary to distort the molecules are largely identical. Instead, the main factor that stabilizes certain motifs over others is the assembly of the single molecules into a free-standing monolayer, i.e. the intermolecular interaction energy. In particular, the most stable conformation with planar molecules arranged in a herringbone pattern benefits from the smallest intermolecular Coulomb repulsion combined with a high van-der-Waals attraction arising from an increased packing density. The most negative adsorption energy for the planar molecules arranged in a herringbone pattern further stabilizes that conformation. These results suggest that the most promising strategy for tuning the molecular conformation in self-assembled monolayer is to modify intra-molecular charge distributions, for example, through electron withdrawing/donating substituents or via the inclusion of heterocyclic rings. The latter strategy has the particular appeal

that it would typically not result in detrimental steric effects, which more or less bulky substituents might cause.

Supplementary Material

Supplementary Material available online, containing (i) a comparison between the energies for different slab thicknesses, (ii) a detailed explanation of the setup for the starting points, (iii) computational details and analysis of the vibrational calculations. Moreover, the Supporting information contains detailed information for the different bonding contributions, applied to each of the two molecules in the unit cell separately and surface band structures for all polymorphs found in this study.

ACKNOWLEDGEMENTS

Many thanks to Dr. Tomáš Bučko for implementing density-functional perturbation-theory (DFPT) including vdW-corrections into our modified VASP version. Funding through the FWF via the projects P27868-N36 and P24666-N20 is gratefully acknowledged. The computational results presented have been achieved using the Vienna Scientific Cluster (VSC).

REFERENCES

- ¹ H. Chung and Y. Diao, *J. Mater. Chem. C* **4**, 3915 (2016).
- ² E. Margapoti, J. Li, Ö. Ceylan, M. Seifert, F. Nisic, T.L. Anh, F. Meggendorfer, C. Dragonetti, C.-A. Palma, J.V. Barth, and J.J. Finley, *Adv. Mater.* 1426 (2015).
- ³ C.-H. Kim, H. Hlaing, J.-A. Hong, J.-H. Kim, Y. Park, M.M. Payne, J.E. Anthony, Y. Bonnassieux, G. Horowitz, and I. Kymissis, *Adv. Mater. Interfaces* 1400384 (2014).
- ⁴ N. Crivillers, S. Osella, C. Van Dyck, G.M. Lazzerini, D. Cornil, A. Liscio, F. Di Stasio, S. Mian, O. Fenwick, F. Reinders, M. Neuburger, E. Treossi, M. Mayor, V. Palermo, F. Cacialli, J. Cornil, and P. Samorì, *Adv. Mater.* **25**, 432 (2013).
- ⁵ L. Newton, T. Slater, N. Clark, and A. Vijayaraghavan, *J. Mater. Chem. C* **1**, 376 (2013).
- ⁶ M. Halik and A. Hirsch, *Adv. Mater.* **23**, 2689 (2011).
- ⁷ H. Ma, H.-L. Yip, F. Huang, and A.K.-Y. Jen, *Adv. Funct. Mater.* **20**, 1371 (2010).
- ⁸ P. Marmont, N. Battaglini, P. Lang, G. Horowitz, J. Hwang, A. Kahn, C. Amato, and P. Calas, *Org. Electron.* **9**, 419 (2008).
- ⁹ F.P. Zamborini and R.M. Crooks, *Langmuir* **14**, 3279 (1998).
- ¹⁰ C.J. Ackerson, P.D. Jadzinsky, J.Z. Sexton, D.A. Bushnell, and R.D. Kornberg, *Bioconjug. Chem.* **21**, 214 (2010).
- ¹¹ T. Wink, S.J. van Zuilen, A. Bult, and W.P. van Bennekom, *Analyst* **122**, 43R (1997).
- ¹² A.M. Hiszpanski, R.M. Baur, B. Kim, N.J. Tremblay, C. Nuckolls, A.R. Woll, and Y.-L. Loo, *J. Am. Chem. Soc.* **136**, 15749 (2014).
- ¹³ W. Azzam, B.I. Wehner, R.A. Fischer, A. Terfort, and C. Wöll, *Langmuir* **18**, 7766 (2002).
- ¹⁴ N. Garg, E. Carrasquillo-Molina, and T.R. Lee, *Langmuir* **18**, 2717 (2002).
- ¹⁵ E.G. Emberly and G. Kirczenow, *Phys. Rev. B* **64**, 235412 (2001).

- ¹⁶ P.E. Kornilovitch and A.M. Bratkovsky, *Phys. Rev. B* **64**, 195413 (2001).
- ¹⁷ T. Ishida, W. Mizutani, N. Choi, U. Akiba, M. Fujihira, and H. Tokumoto, *J. Phys. Chem. B* **104**, 11680 (2000).
- ¹⁸ T.Y.B. Leung, P. Schwartz, G. Scoles, F. Schreiber, and A. Ulman, *Surf. Sci.* **458**, 34 (2000).
- ¹⁹ R. Naaman, A. Haran, A. Nitzan, D. Evans, and M. Galperin, *J. Phys. Chem. B* **102**, 3658 (1998).
- ²⁰ Y.-T. Tao, C.-C. Wu, J.-Y. Eu, W.-L. Lin, K.-C. Wu, and C. Chen, *Langmuir* **13**, 4018 (1997).
- ²¹ A. Bashir, E. Sauter, N. Al-Refaie, M. Rohwerder, M. Zharnikov, and W. Azzam, *ChemPhysChem* **18**, 702 (2017).
- ²² A. Bashir, W. Azzam, M. Rohwerder, and A. Terfort, *Langmuir* **29**, 13449 (2013).
- ²³ N. n. Sirota, *Cryst. Res. Technol.* **17**, 661 (1982).
- ²⁴ T. Bučko, J. Hafner, and J.G. Ángyán, *J. Chem. Phys.* **122**, 124508 (2005).
- ²⁵ P. Cyganik, M. Buck, W. Azzam, and C. Wöll, *J. Phys. Chem. B* **108**, 4989 (2004).
- ²⁶ E. Verwüster, O.T. Hofmann, D.A. Egger, and E. Zojer, *J. Phys. Chem. C* **119**, 7817 (2015).
- ²⁷ N. Meyerbroeker, P. Waske, and M. Zharnikov, *J. Chem. Phys.* **142**, 101919 (2015).
- ²⁸ Y. Carissan and W. Klopper, *J. Mol. Struct. THEOCHEM* **940**, 115 (2010).
- ²⁹ G. Heimel, F. Rissner, and E. Zojer, *Adv. Mater.* **22**, 2494 (2010).
- ³⁰ L. Wang, G.M. Rangger, L. Romaner, G. Heimel, T. Bučko, Z. Ma, Q. Li, Z. Shuai, and E. Zojer, *Adv. Funct. Mater.* **19**, 3766 (2009).
- ³¹ Q. Sun and A. Selloni, *J. Phys. Chem. A* **111**, 10170 (2007).
- ³² G. Heimel, L. Romaner, J.-L. Brédas, and E. Zojer, *Surf. Sci.* **600**, 4548 (2006).
- ³³ Q. Sun, A. Selloni, and G. Scoles, *J. Phys. Chem. B* **110**, 3493 (2006).
- ³⁴ T.Y.B. Leung, P. Schwartz, G. Scoles, F. Schreiber, and A. Ulman, *Surf. Sci.* **458**, 34 (2000).

- ³⁵ U. Kleineberg, A. Brechling, M. Sundermann, and U. Heinzmann, *Adv. Funct. Mater.* **11**, 208 (2001).
- ³⁶ J.F. Kang, S. Liao, R. Jordan, and A. Ulman, *J. Am. Chem. Soc.* **120**, 9662 (1998).
- ³⁷ M.O. Sinnokrot and C.D. Sherrill, *J. Phys. Chem. A* **110**, 10656 (2006).
- ³⁸ M.O. Sinnokrot, E.F. Valeev, and C.D. Sherrill, *J. Am. Chem. Soc.* **124**, 10887 (2002).
- ³⁹ T. Dahl, *Acta Chem. Scand.* **48**, 95 (1994).
- ⁴⁰ C.A. Hunter and J.K.M. Sanders, *J. Am. Chem. Soc.* **112**, 5525 (1990).
- ⁴¹ C.A. Hunter, J. Singh, and J.M. Thornton, *J. Mol. Biol.* **218**, 837 (1991).
- ⁴² G. Kresse and J. Furthmüller, *Phys. Rev. B* **54**, 11169 (1996).
- ⁴³ J.P. Perdew, K. Burke, and M. Ernzerhof, *Phys. Rev. Lett.* **77**, 3865 (1996).
- ⁴⁴ J.P. Perdew, K. Burke, and M. Ernzerhof, *Phys. Rev. Lett.* **78**, 1396 (1997).
- ⁴⁵ G. Kresse and D. Joubert, *Phys. Rev. B* **59**, 1758 (1999).
- ⁴⁶ P. Blöchl, *Phys. Rev. B* **50**, 17953 (1994).
- ⁴⁷ A. Tkatchenko and M. Scheffler, *Phys. Rev. Lett.* **102**, 073005 (2009).
- ⁴⁸ V.G. Ruiz, W. Liu, E. Zojer, M. Scheffler, and A. Tkatchenko, *Phys. Rev. Lett.* **108**, 146103 (2012).
- ⁴⁹ H.J. Monkhorst and J.D. Pack, *Phys. Rev. B* **13**, 5188 (1976).
- ⁵⁰ J. Neugebauer and M. Scheffler, *Phys. Rev. B* **46**, 16067 (1992).
- ⁵¹ T.P. Hamilton and P. Pulay, *J. Chem. Phys.* **84**, 5728 (1986).
- ⁵² M.J. Frisch, G.W. Trucks, H.B. Schlegel, G.E. Scuseria, M.A. Robb, J.R. Cheeseman, G. Scalmani, V. Barone, B. Mennucci, G.A. Petersson, H. Nakatsuji, M. Caricato, X. Li, H.P. Hratchian, A.F. Izmaylov, J. Bloino, G. Zheng, J.L. Sonnenberg, M. Hada, M. Ehara, K. Toyota, R. Fukuda, J. Hasegawa, M. Ishida, T. Nakajima, Y. Honda, O. Kitao, H. Nakai, T. Vreven, J.A.

Montgomery Jr., J.E. Peralta, F. Ogliaro, M. Bearpark, J.J. Heyd, E. Brothers, K.N. Kudin, V.N. Staroverov, R. Kobayashi, J. Normand, K. Raghavachari, A. Rendell, J.C. Burant, S.S. Iyengar, J. Tomasi, M. Cossi, N. Rega, J.M. Millam, M. Klene, J.E. Knox, J.B. Cross, V. Bakken, C. Adamo, J. Jaramillo, R. Gomperts, R.E. Stratmann, O. Yazyev, A.J. Austin, R. Cammi, C. Pomelli, J.W. Ochterski, R.L. Martin, K. Morokuma, V.G. Zakrzewski, G.A. Voth, P. Salvador, J.J. Dannenberg, S. Dapprich, A.D. Daniels, Ö. Farkas, J.B. Foresman, J.V. Ortiz, J. Cioslowski, and D.J. Fox, *Gaussian09, Revision D.01*.

⁵³ F. Grein, *J. Phys. Chem. A* **106**, 3823 (2002).

⁵⁴ P. Puschnig, K. Hummer, C. Ambrosch-Draxl, G. Heimel, M. Oehzelt, and R. Resel, *Phys. Rev. B* **67**, 235321 (2003).

⁵⁵ C.B. Pinheiro and A.M. Abakumov, *IUCrJ* **2**, 137 (2015).

⁵⁶ O. Potzel and G. Taubmann, *Phys. Chem. Chem. Phys.* **15**, 20288 (2013).

⁵⁷ A.T.H. Lenstra, C. Van Alsenoy, K. Verhulst, and H.J. Geise, *Acta Crystallogr. B* **50**, 96 (1994).

⁵⁸ G.-P. Charbonneau and Y. Delugeard, *Acta Crystallogr. B* **32**, 1420 (1976).

⁵⁹ W. Azzam, C. Fuxen, A. Birkner, H.-T. Rong, M. Buck, and C. Wöll, *Langmuir* **19**, 4958 (2003).

⁶⁰ A.-A. Dhirani, R.W. Zehner, R.P. Hsung, P. Guyot-Sionnest, and L.R. Sita, *J. Am. Chem. Soc.* **118**, 3319 (1996).

⁶¹ S. Frey, V. Stadler, K. Heister, W. Eck, M. Zharnikov, M. Grunze, B. Zeysing, and A. Terfort, *Langmuir* **17**, 2408 (2001).

⁶² J. Poater, M. Solà, and F.M. Bickelhaupt, *Chem. – Eur. J.* **12**, 2889 (2006).

⁶³ M.P. Johansson and J. Olsen, *J. Chem. Theory Comput.* **4**, 1460 (2008).

⁶⁴ A. Almenningen, O. Bastiansen, L. Fernholt, B.N. Cyvin, S.J. Cyvin, and S. Samdal, *J. Mol. Struct.* **128**, 59 (1985).

- ⁶⁵ J. Trotter, *Acta Crystallogr.* **14**, 1135 (1961).
- ⁶⁶ M.P. Johansson and J. Olsen, *J. Chem. Theory Comput.* **4**, 1460 (2008).
- ⁶⁷ E. Sauter, G. Nascimbeni, S. Ludwigs, F. von Wrochem, and M. Zharnikov, *in preparation*.
- ⁶⁸ S. Tsuzuki, T. Uchimaru, K. Matsumura, M. Mikami, and K. Tanabe, *Chem. Phys. Lett.* **319**, 547 (2000).
- ⁶⁹ D.E. Williams and Y. Xiao, *Acta Crystallogr. A* **49**, 1 (1993).
- ⁷⁰ L. Wang, G.M. Rangger, Z. Ma, Q. Li, Z. Shuai, E. Zojer, and G. Heimel, *Phys. Chem. Chem. Phys.* **12**, 4287 (2010).
- ⁷¹ K. Tonigold and A. Groß, *J. Chem. Phys.* **132**, 224701 (2010).
- ⁷² A. M. Track, F. Rissner, G. Heimel, L. Romaner, D. Käfer, A. Bashir, G. M. Rangger, O. T. Hofmann, T. Bučko, G. Witte, and E. Zojer, *J. Phys. Chem. C* **114**, 2677 (2010).
- ⁷³ J. Nara and S. Higai, *J. Chem. Phys.* **120**, 6705 (2004).
- ⁷⁴ S. Liao, Y. Shnidman, and A. Ulman, *J. Am. Chem. Soc.* **122**, 3688 (2000).